Hyperthermia System Based on Extrinsically Magnetic Poly (Butylene Succinate)

*Rafael S. Moraes, Vivian Saez, José A. R. Hernandez, and Fernando G. de Souza Júnior**

In this work, an extrinsically magnetic composite based on modified magnetite and poly (butylene succinate) (PBS) is prepared. The magnetic composite is obtained by the emulsion–solvent evaporation method. Several analytical tests confirm the synthesis of the composites. Among them, Nuclear magnetic resonance (NMR) results in comparison with literature confirms the synthesis of PBS. X-Ray Diffraction (XRD) shows the characteristic peaks of PBS, in its monoclinic structure. The crystallite size (Lc) of magnetic particles inside the composite, is equal to 13 nm. Thermogravimetric analysis (TGA) reveals the presence of 5.3 wt% magnetite in the composite and demonstrates that the inclusion of magnetite does not affect the thermal stability of the polymer. The analysis of Fourier transform infrared attenuated total reflection spectra (FTIR-ATR) indicates the synthesis of desired products as well as the encapsulation of magnetite in PBS polymer matrix. The composite presents magnetic force, which allows its magnetic guidance to a target area. Besides, the magnetic induction heating test promotes heating within the therapeutic range from 40 to 45 °C, being able, according to literature, to promote the death of several types of cancer's cells. Therefore, the material here presented possesses potential to be deeply researched as a future cancer treatment tool.

1. Introduction

Cancer is the second largest cause of death in the world. There are 14 million new cases registered by year, and the World Health Organization predicts that the number of cases will increase 100% in two decades.[1]

The most common treatments are surgeries, specific medications, and ionizing radiation. The combination of these techniques is also used. However, each one of these cancer treatments produces substantial side effects. The side effects are due to the low cytoselectivity of these agents, attacking the patient's healthy cells as well.[2]

Thus, new and more effective cancer treatments are always being pursued. Among them, the hyperthermia is one of the most promising. This technique consists in heating the tumor cells, increasing their sensitivity to other treatments, as well as leading them to death. As the tumor cells are considerably less resistant to heat than the surrounding healthy cells, the hyperthermia treatment is cytoselective, producing fewer side effects in comparison to classic treatment of neoplasms.[3–7]

Hyperthermia machine has already been approved by the United States Food and Drug Administration for single or associated treatment against solid tumors.[8–11] Also, several specialized centers in Germany use this technique (e.g., St. Georg Hospital[12] and the Hannover Hyperthermia Center[13]) extensively.

Among the possible ways of promoting hyperthermia, magnetohyperthermia is preferred since produces few side effects, avoiding promote warmth of the surrounding healthy tissue.[14] This preservation of the healthy tissues is possible because nanocomposites are inside the tumor. Then, when subjected to a magnetic field, only the tumor will be affected by the temperature increase.[15,16] Thus, in this specific context, the use of magnetic nanoparticles to damage cancerous tissues is called magnetothermal cytolysis.

Metal nanoparticles possess low zeta potential values,[17] presenting a strong tendency to agglomeration, reducing their desirable magnetic properties. Besides that, for clinical use, they should be covered with some biocompatible material, which helps in its colloidal stability without harming its magnetic properties. For this, polymeric coatings, such as poly-3-hydroxybutyrate[18] and polylactic acid,[19] have been used. Other polymers, like poly (butylene succinate), can also be exploited for this application. PBS has excellent biocompatibility[20] and

R. S. Moraes, V. Saez, F. G. de Souza Júnior
Instituto de Macromoléculas
Centro de Tecnologia-Cidade Universitária
Bloco J. Universidade Federal de Rio de Janeiro
Av. Horacio Macedo, 2030, Rio de Janeiro 21941-909, Brasil
E-mail: fgsj@ufrj.br

J. A. R. Hernandez
Escola de Química
Centro de Tecnologia-Cidade Universitária
Bloco E. Universidade Federal deRio de Janeiro
av. Horacio Macedo, 2030, Rio de Janeiro, Brasil

F. G. de Souza Júnior
Programa de Engenharia Civil
COPPE, Centro de Tecnologia-Cidade Universitária
Bloco I. Universidade Federal de Rio de Janeiro
Av. Horacio Macedo, 2030, Rio de Janeiro 21941-914, Brasil

DOI: 10.1002/masy.201800108

bioabsorption[21] characteristics. Also, PBS is recognized as a renewable and biodegradable alternative for biomedical and pharmaceutical applications.[22–25] Surface modification of metal nanoparticles can contribute to increase zeta potential, improving colloidal stability and avoiding agglomeration. Consequently, smaller particles will be encapsulated by the polymer, resulting in smaller sizes of the composite. Succinic acid was chosen for that purpose because of its easy interaction with the iron hydroxide in the surface layers of the magnetite and its biocompatibility. To the best of our knowledge, PBS has never been used for this objective.

So, this work aimed to synthesize a magnetic composite consisting of magnetite nanoparticles modified with succinic acid and encapsulated in PBS with potential application in magnetohyperthermia. The obtained materials were studied using several characterization techniques and the obtained the results allow us to consider the composite obtained as promising for a possible treatment by magnetohyperthermia.

2. Experimental Section

2.1. Materials

Succinic acid P.A (99.0%), ferric chloride hexahydrate (99.0%), potassium hydroxide (99.0%), ferrous sulfate heptahydrate (99%), 1,4-butanediol P.S (99.3%), sulfuric acid (95–99%), ethyl alcohol, silicone bath, dichloromethane (99%), silicone grease for high vacuum, and titanium butoxide ($Ti(OBu)_4$). All reactants were purchased from Sigma-Aldrich, St. Luis Missouri, USA. And used as received.

2.2. Methods

2.2.1. Poly(Butylene Succinate) Synthesis

Equimolar amounts of 1,4-butanediol (27 mL) and succinic acid (35.9 g) and 0.1 mL of sulfuric acid were used. The system was

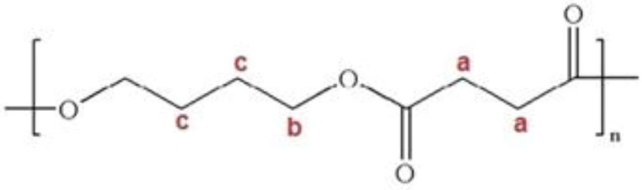

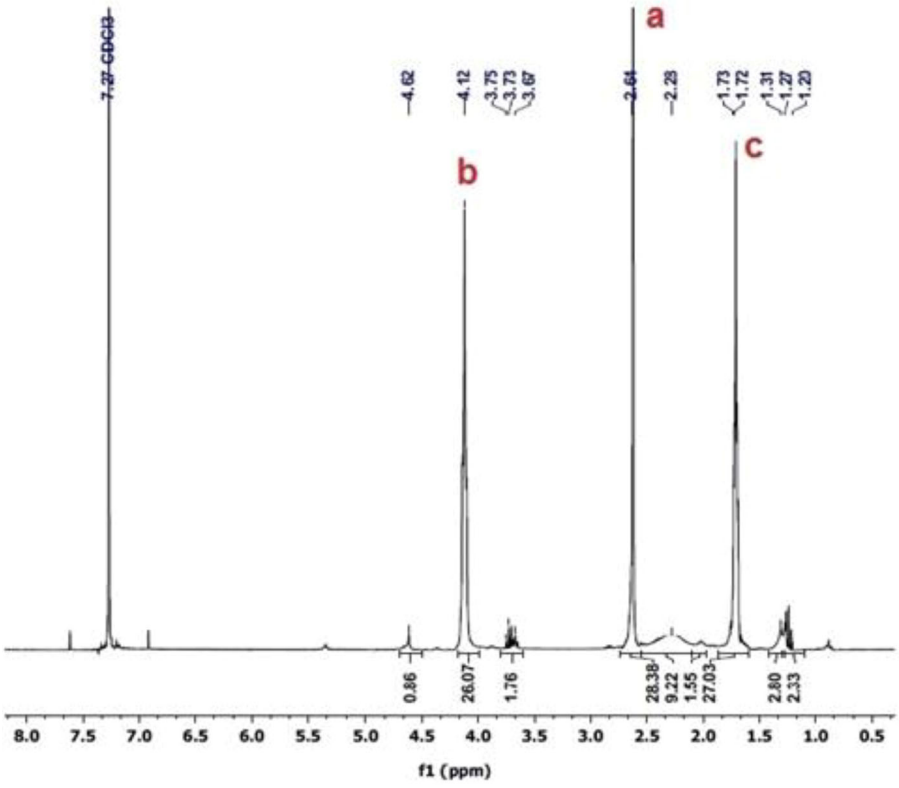

Figure 1. 1H-NMR spectrum of PBS.

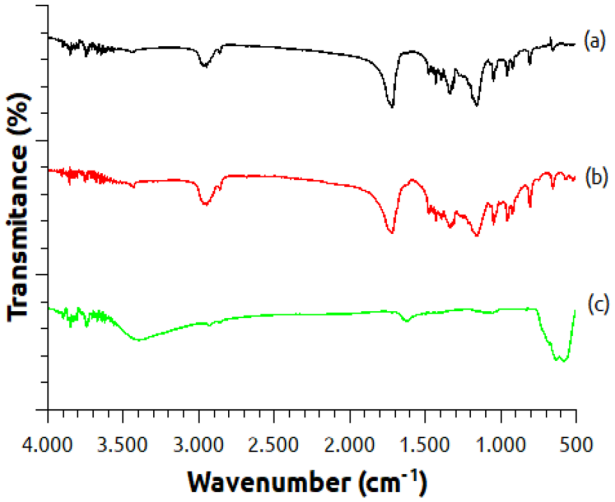

Figure 2. FTIR-ATR spectra of PBS (a), magnetic composite (b) and magnetite (c).

assembled using a heating plate under vacuum and nitrogen flow. At the outlet of the condenser, a flask was placed under ice bath, and the trap was cooled using liquid nitrogen. After heating at 135 °C for 6 h, the catalyst tetrabutoxytitanium (Ti (OBu) 4) 0.1%, was added and the temperature gradually raised to 200 °C. These conditions were kept for 12 h. The product of the synthesis was dissolved in dichloromethane, and mixed with an excess of ethanol in an ice bath, forcing its precipitation. The precipitate was washed with ethanol and dried under vacuum for 24 h.[26]

2.2.2. Magnetite Synthesis

Magnetic nanoparticles were prepared as reported elsewhere.[3,26–39] Ferric chloride hexahydrate (6.75 g) and ferrous sulfate heptahydrate (6.95 g) were dissolved in 30 mL of deionized water. An aqueous 0.112 g mL^{-1} solution of potassium hydroxide was added to this solution and then mechanically stirred for 30 min.

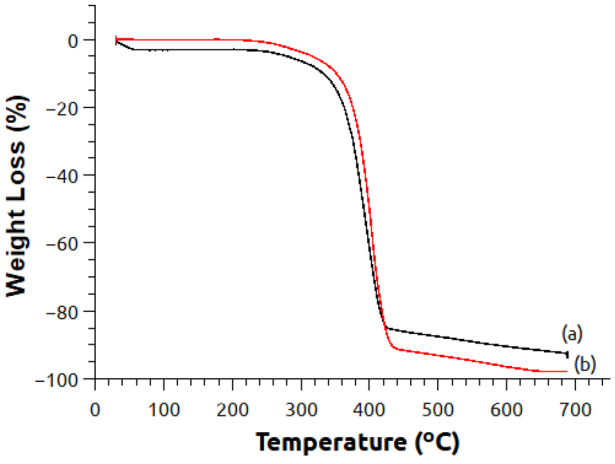

Figure 3. TGA curve of magnetite composite (a) and PBS (b).

The precipitate was washed with distilled water to neutral pH and lyophilized. The powder was macerated and sifted through a 75-micron sieve to obtain a homogeneous material.

2.2.3. Magnetite Modification

Magnetite (5 g) was dispersed in 150 mL of distilled water at 60 °C by mechanical stirring. The suspension was placed under a nitrogen atmosphere, and 20 mL of aqueous solution 0.01 g mL^{-1} of succinic acid was dropped slowly on the medium. The dispersion was stirred for 1 h. Then, it was frozen and freeze-dried.[26]

2.2.4. Composite Preparation

Modified magnetite nanoparticles (10 mg) were dispersed in 5 mL of PBS solution (10 wt%) of PBS in dichloromethane) by means of a high-shear homogenizer (Ultra Turrax T-10, IKA, USA) This dispersion was added to 50 mL of polyvinyl alcohol (PVA) (0.5 wt% of PVA in distilled water) previously placed in an ice bath. The system was agitated at 14,000 rpm during 3 min for emulsification using the Ultra Turrax T-10. The emulsion was poured into a beaker with 400 mL of 0.1% PVA aqueous solution and kept under stirring using a mechanical stirrer at 300 rpm for solvent evaporation. The composite suspension was decanted and the non-encapsulated bigger magnetic particles were removed by fixing them at the bottom of the beaker with an imam. Composite particles were then precipitated by centrifugation, washed three times with distilled water and lyophilized (Liotop L101, Liobras, Brazil).

2.3. Material Characterization

2.3.1. Attenuated Total Reflectance with Fourier Transform Infrared Spectroscopy (FTIR-ATR)

The samples of PBS, magnetite and the composite were analyzed by FTIR. The spectra of the samples were obtained using an Excalibur Varian 3100 FTIR spectrometer (Varian, USA). The spectra were collected between 4000 and 550 cm^{-1}, using an attenuated total reflection (ATR) accessory with a ZnSe crystal. Non-additional sample preparation was required. The resolution was 4 cm^{-1}, and 120 scans were used to compose each spectrum.

2.3.2. Thermogravimetric Analysis (TGA)

Samples of PBS, magnetite, and composite were submitted to thermogravimetric analysis. The heating ramp method was used, with a nitrogen atmosphere, ranging from 25 °C to 700 °C. Samples were characterized using a TA Instruments Q500 V6.7 Build 203 analyzer. Measurements were carried out in nitrogen at a heating rate of 20 °C min^{-1} with a gas flow rate of 20 mL min^{-1}.

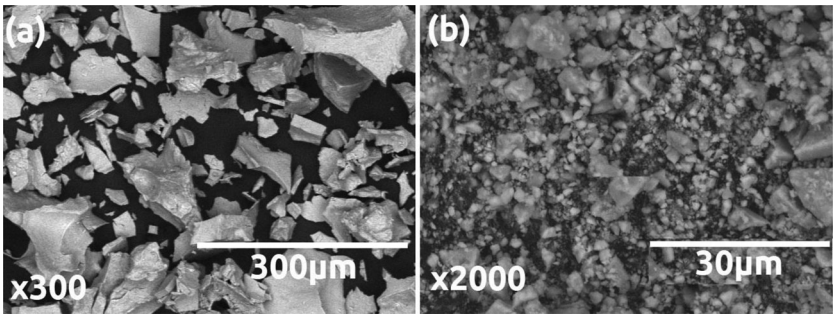

Figure 4. SEM micrographs of the magnetite without modification (a) and with modification (b).

2.3.3. Scanning Electron Microscopy (SEM)

To observe the morphology of the magnetite nanoparticles and the composite, SEM micrographs were analyzed. A JEOL JSL 5300 Microscope (Jeol Instruments, Japan) was used, operating in 5 keV. The samples were covered with gold. For the determination of the average size of the composite beads, the pixel count was used through the software Image J. The size was determined by the average of 23 measurements of diameters of composites with excellent definition and all their visible extension. The measurements were performed in triplicate, and the final result is the arithmetic mean of them.

2.3.4. X-Ray Diffraction (XRD)

The samples were submitted to XRD test. The analyzes were performed varying the 2θ angle from 2° to 50° by the fixed time method, at 0.05° per second, using Cu Kα radiation, length of 1.5418Å, at room temperature. The used equipment was a multipurpose X-ray diffraction diffractometer Ultima IV from Rigaku Inc, model Miniflex. The crystallite size (Lc) was calculated using the Scherrer's Equation (1),

$$\mathrm{Lc} = \frac{k\lambda}{\beta \cos\theta} \tag{1}$$

where k is the proportionality constant as a function of morphology, λ is the wavelength of Cu Kα (1.5406Å), and β is the width at half height of the peak.

2.3.5. Nuclear Magnetic Resonance (NMR)

For the determination of the polymer structure, the NMR was performed using the 300 MHz Spectrometer (Varian Mercury 300, USA) – High-Resolution Nuclear Magnetic Resonance (NMR) frequency of 23.4 MHz, with a probe of 18 mm at a temperature of 30 °C, with a 90° pulse of 3.0 μs.

2.3.6. Magnetic Force Test

Magnetic force tests were performed using a home-made experimental setup, described elsewhere.[40] This setup is constituted by an analytical balance Shimadzu AY-220, a voltage source ICEL PS-4100, a digital multimeter ICEL MD-6450, a gaussmeter GlobalMag TLMP-Hall-02; a home-made sample holder and a home-made electromagnet. System calibration was performed in the absence of magnetic material. First, using the amperemeter and the gaussmeter, a current versus magnetic field calibration was performed. Soon afterward a current versus mass calibration was also performed. Obtained results were used to predict part of the presented error. Magnetic force tests were performed following the mass variation of the sample in the presence of the magnetic field, produced by the electromagnet. Then, the apparent variation of mass of the sample in the presence of magnetic field was calculated by subtracting the mass of the sample in the presence of magnetic field from the mass of the sample. The magnetic force (opposite to gravitational one) was calculated according to Equation (2):

$$\mathrm{Fm}_n = \frac{\Delta m x g}{m_0} \tag{2}$$

where Fm_n is the magnetic force normalized by the initial mass of the sample m_0, Δm is the apparent variation of mass in the presence of the magnetic field, and g is the acceleration of gravity.

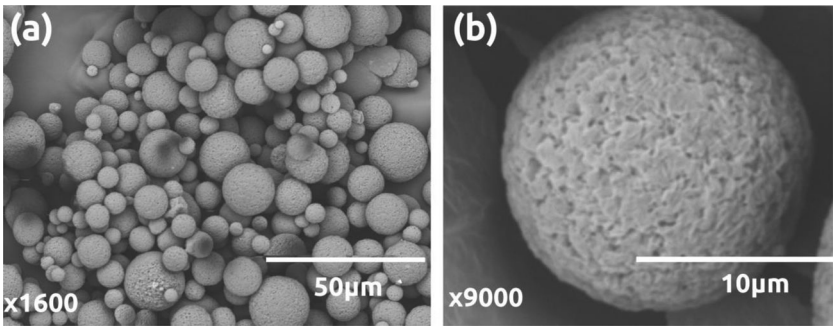

Figure 5. SEM micrographs of the composite particles (a) and superficial details (b).

2.3.7. Magnetic Induction Heating Test

The test was performed aiming to investigate the potential of magnetic nanoparticles for applications in hyperthermia. A dispersion of 20 mg of the composite in 2 mL of water was prepared. This system was placed in the magnetic inductor coil (Ambrell

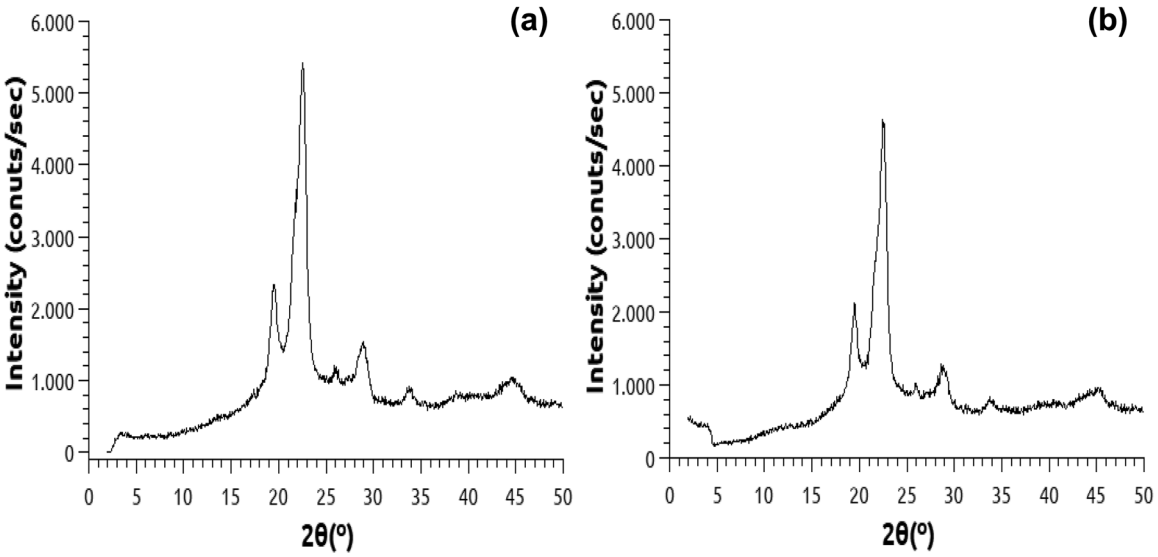

Figure 6. Diffractogram of PBS (a) and composite (b).

EASYHEAT machine model L1. Samples) and subjected to the magnetic field alternated produced by electrical currents of 600A and frequency of 220 kHz. The temperatures were measured using a thermocouple. The specific absorption rate (SAR) was used to evaluate the heating potential of magnetic material when exposed to an alternating magnetic field. The SAR value was calculated according to the following Equation (3):

$$\mathrm{SAR} = \left[C_{\mathrm{np}} + \frac{p_{\mathrm{H2O}} \times C_{\mathrm{H2O}}}{p_{\mathrm{np}}} \right] \times \frac{\Delta_T}{\Delta_t} \quad (3)$$

where C_{np} is nanoparticles specific heat (0.161 cal.g^{-1}.°C^{-1}), p_{H2O} is water density (1000 mg mL^{-1}), C_{H2O} is water specific heat (1.000 cal.g^{-1}.°C^{-1}), p_{np} is the concentration of the particles (20 mg mL^{-1}) and $\Delta T/\Delta t$ is the slope of the heating curve.

3. Results and Discussion

Figure 1 shows the NMR for hydrogen atoms in the PBS sample. The chemical shift at 2.61 ppm (a) is due to the methylene protons present in the succinic acid units. In turn, the peaks centered at 4.12 (b) and 1.72 ppm (c) are due to the methylene protons from 1,4-butanediol. These results are in agreement with literature and confirm the synthesis of PBS.[41]

The FTIR-ATR spectra of magnetite, polymer, and composite are shown in **Figure 2**. The two main characteristic bands of the magnetite[42–45] were observed. They are the band

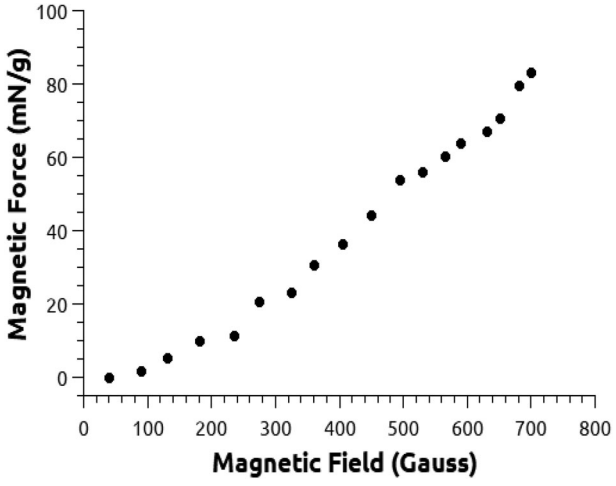

Figure 7. Magnetic force of the composite in response to the applied magnetic field.

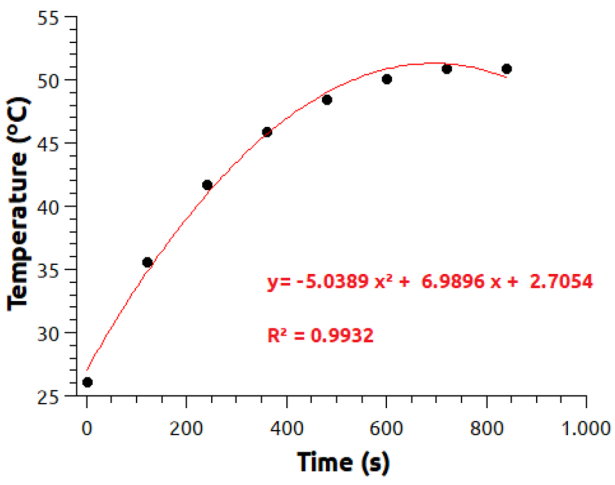

Figure 8. Heating of the composite under application of an alternating magnetic field.

centered at 3455 cm^{-1}, related to the stretch of the O-H group of the FeOH surface and the one centered at 571 cm^{-1}, which is from Fe-O bond vibration. The characteristic bands of PBS were observed.[46,47] Among them, the one centered at 1044 cm^{-1} corresponds to the elongation of the O—C—C bonds of PBS. The bands around 1140 and 1264 cm^{-1} are related to the C—O—C— stretch of the ester group of PBS. The bands around 1330 and 2945, 2964, 2968 cm^{-1} are due to the symmetrical and asymmetrical axial strain deformations of the $-CH_2-$ groups in the main polymer chain. The bands centered at 1714 cm^{-1} and 3453 cm^{-1} are referred to the elongation of the C═O carbonyl group. Composites presented these main bands. On the other hand, composites did not present the magnetite bands, mainly because PBS encapsulates these nanoparticles.

The thermogravimetric tests of the materials are shown in **Figure 3**. PBS presented a residue equal to 2.2 wt%, compatible with the expected residue from an organic material tested in the nitrogen atmosphere. The thermogravimetric analysis of the polymer and composite materials showed similar onset temperatures, demonstrating that the presence of magnetite does not affect the thermal stability of the polymer. The presence of a residual mass of 7.4 wt% when compared to the pure polymer residue indicates the presence of 5.3 wt% magnetite in the composite.

Scanning electron microscopy tests were performed, and results are shown in **Figure 4** and 5. Figure 4 shows the magnetite with and without surface modification with succinic acid. It can be observed that the modification produced smaller particles with smoother surface. Micrograph shows a wide particle size distribution, however only the smaller particles were encapsulated by the polymer matrix.

Figure 5 proves that spherical particles of the composite were obtained. The particles exhibited a rough surface with some pores. The absence of magnetite particles in the micrograph corroborates the FTIR-ATR results, proving that magnetic particles are trapped inside the PBS. The average diameter of the spheres was equal to $(12 \pm 3)\mu m$, being adequate for biomedical applications which do not include embolization.[48]

As can be seen in the micrograph, the composite presents a considerable dispersion of sizes ranging from 2 to 20 μm. For biomedical applications, a narrower range of sizes is desirable. For this, optimizations in the synthesis and separation of the sizes may be necessary.

The diffractograms of PBS and composite are shown in **Figure 6**.

Figure 6a shows the characteristic peaks of a polymer monoclinic crystal structure, with 2θ peaks centered at 19.6°; 21.9°; 22.7°; 28.9° and 44.8°. The composite, shown in Figure 6b presented an additional peak, centered at 35.7°. This peak was used to calculate the crystallite size (Lc) of magnetic particles inside the composite. The obtained result was equal to 13 nm. Therefore, the produced material, as proved elsewhere,[3,27,29–31,33–39,49–55] can be classified as a nanocomposite.

As also proved elsewhere, magnetic force values higher than 600 mN g^{-1} are considered as suitable for practical applications.[34] As shown in **Figure 7**, the magnetic nanoparticles here prepared presented magnetic force equal to 973 mN g^{-1} @700 Gauss. In turn, the composite material presented a magnetic force equal to 82 mN g^{-1} @700 Gauss. Therefore, the magnetic force is proportional to the amount of magnetite within the composite previously determined by TGA.

Finally, the magnetic induction heating test was performed, and the results are shown in **Figure 8**. For hyperthermia, materials with high SAR values are adequate, because less quantity of material is needed to promote the same heat. As a result, the insertion of lower mass of material is needed to treat the patient, reducing the chances of toxicity.

The specific absorption rate (SAR) of the composite sample was equal to 32,029 W kg^{-1}. This value is comparable to the one reported by Gloover et al.[56] for iron oxide nanoparticles applied to hyperthermia, being the material presented here potentially able to destroy cancer cells. Besides that, the therapeutic temperature, 43–45 °C[57–59] was reached about 400 s. This small-time needed to reach the therapeutic temperature is attractive to the treatment, could increase the success of the procedure.[60]

4. Conclusions

Magnetite particles synthesized by the alkaline co-precipitation method and modified with succinic acid could be encapsulated in poly (butylene succinate) microspheres by the emulsion – solvent evaporation method. The particulate composite presents a spherical morphology and a magnetic force which can produce the elevation of the temperature up to the therapeutic level. These characteristics make this system adequate for potential application in magnetohyperthermia. Future works will be focused on the decrease in composite size dispersion and co-encapsulation of an anticancer drug aiming to produce a treatment able to join multiples techniques.

Acknowledgements

The authors thank the Conselho Nacional de Desenvolvimento Científico e Tecnológico (CNPq-474940/2012-8 and 550030/2013-1), Coordenação de Aperfeiçoamento de Pessoal de Nível Superior (CAPES and CAPES-MES Cuba # 133–11 and 154/12), Financiadora de Estudos e Projetos (FINEP PRESAL Ref.1889/10) and Fundação Carlos Chagas Filho de Amparo à Pesquisa do Estado do Rio de Janeiro (FAPERJ) for the financial support and scholarships.

Keywords

cancer, hyperthermia, induction heating, magnetic composite

[1] B. W. Stewart, C. P. Wild, World Cancer Report 2014, International Agency for Research on Cancer/World Health Organization, Lyon 2014.
[2] A. Schroeder, D. A. Heller, M. M. Winslow, J. E. Dahlman, G. W. Pratt, R. Langer, T. Jacks, D. G. Anderson, *Nat. Rev. Cancer* **2012**, *12*, 39.
[3] F. G. Souza, Jr., J. A. Marins, C. H. M. Rodrigues, J. C. Pinto, *Macromol. Mater. Eng.* **2010**, *295*, 942.
[4] E. D. Pereira, R. Cerruti, E. Fernandes, L. Peña, V. Saez, J. C. Pinto, J. A. Ramón, G. E. Oliveira, F. G. Souza, Jr., *Polímeros* **2016**, 0.

[5] J. W. Strohbehn, E. B. Douple, *IEEE Trans. Biomed. Eng.* **1984**, *BME-31*, 779.
[6] S. Laurent, S. Dutz, U. O. Häfeli, M. Mahmoudi, *Adv. Colloid Interface Sci.* **2011**, *166*, 8.
[7] J. Beik, Z. Abed, F. S. Ghoreishi, S. Hosseini-Nami, S. Mehrzadi, A. Shakeri-Zadeh, S. K. Kamrava, *J. Controlled Release* **2016**, *235*, 205.
[8] Inc, P. M., "Humanitarian Device Exemption (HDE)," can be found under https://www.accessdata.fda.gov/scripts/cdrh/cfdocs/cfhde/hde.cfm?id = H090002, **2018**.
[9] J. van der Zee, *Ann. Oncol.* **2002**, *13*, 1173.
[10] K. Mahmoudi, A. Bouras, D. Bozec, R. Ivkov, C. Hadjipanayis, *Int. J. Hyperthermia* **2018**, *0*, 1.
[11] P. Gas, *ArXiv171000656 Phys.* **2017**.
[12] St. George Hospital, *St George Hosp.* n.d.
[13] Hannover Hyperthermia Center, "Metastatic Carcinoma | Pilot Hole – Leading the way," can be found under https://pilothole.org/bronchogenic-carcinoma-lung-cancer/metastatic-carcinoma/, n.d.
[14] M. L. Carneiro, E. S. Nunes, R. C. Peixoto, R. G. Oliveira, L. H Lourenço, I. C. da Silva, A. R. Simioni, A. C. Tedesco, A. R. de Souza, Z. G. Lacava, S. N. Báo, *J. Nanobiotechnology* **2011**, *9*, 11.
[15] H. Chiriac, T. Petreus, E. Carasevici, L. Labusca, D.-D. Herea, C. Danceanu, N. Lupu, *J. Magn. Magn. Mater.* **2015**, *380*, 13.
[16] M. Colombo, S. Carregal-Romero, M. F. Casula, L. Gutiérrez, M. P. Morales, I. B. Böhm, J. T. Heverhagen, D. Prosperi, W. J. Parak, *Chem. Soc. Rev.* **2012**, *41*, 4306.
[17] A. Petri-Fink, M. Chastellain, L. Juillerat-Jeanneret, A. Ferrari, H. Hofmann, *Biomaterials* **2005**, *26*, 2685.
[18] C. Oka, K. Ushimaru, N. Horiishi, T. Tsuge, Y. Kitamoto, *J. Magn. Magn. Mater.* **2015**, *381*, 278.
[19] W. Wu, Q. He, C. Jiang, *Nanoscale Res. Lett.* **2008**, *3*, 397.
[20] H. Wang, J. Ji, W. Zhang, Y. Zhang, J. Jiang, Z. Wu, S. Pu, P. Chu, *Acta Biomater.* **2009**, *5*, 279.
[21] G. G. Santos Dos, S. M. O. Cavalcanti Marinho, F. B. Miguel, *Rev. Ciênc. Médicas E Biológicas* **2013**, *12*, 367.
[22] Y. Ikada, H. Tsuji, *Macromol. Rapid Commun.* **2000**, *21*, 117.
[23] M. Gigli, M. Fabbri, N. Lotti, R. Gamberini, B. Rimini, A. Munari, *Eur. Polym. J.* **2016**, *75*, 431.
[24] L. P. Ferreira, B. P. da Cunha, R. M. Kuster, J. C. Pinto, M. N. Souza, F. G. Souza, Jr., *Ind. Crops Prod.* **2017**, *97*, 599.
[25] F. G. Souza, Jr., D. Soares, R. Freitas, V. Soares, L. Ferreira, J. Ramon, G. E. Oliveira, *Curr. Appl. Polym. Sci.* **2017**, *1*, 1.
[26] R. S. Moraes, N. Ricardo, V. Saez, F. G. de Sousa, *MOJ Polym. Sci.* **2018**, *2*, 00044.
[27] E. U. X. Péres, F. G. Souza, Jr., F. M. Silva, J. A. Chaker, P. A. Z. Suarez, *Ind. Crops Prod* **2014**, *59*, 260.
[28] F. G. Souza, Jr., A. M. da Silva, G. E. de Oliveira, R. M. Costa, E. R. Fernandes, E. D. Pereira, *Ind. Crops Prod.* **2015**, *68*, 97.
[29] R. M. D. Costa da, G. Hungerbühler, T. Saraiva, G. De Jong, R. S. Moraes, E. G. Furtado, F. M. Silva, G. E. Oliveira de, L. S. Ferreira, F. G. Souza, Jr, *Polímeros* **2017**, *27*, 273.
[30] J. S. Neves, F. G. Souza, Jr., P. A. Z. Suarez, A. P. Umpierre, F. Machado, *Macromol. Mater. Eng.* **2011**, *296*, 1107.
[31] E. D. Pereira, F. G. Souza, C. I. Santana, D. Q. Soares, A. S. Lemos, L. R. Menezes, *Polym. Eng. Sci.* **2013**, *53*, 2308.
[32] F. G. Souza, Jr., J. Marins, J. Pinto, G. de Oliveira, C. Rodrigues, L. Lima, *J. Mater. Sci* **2010**, *45*, 5012.
[33] A. Middea, L. Spinelli, F. G. Souza de, Junior, R. Neumann, T. Fernandes, F. R. L. Faulstich, O. Gomes, *J. Appl. Polym. Sci.* **2018**, *135*, 46162.
[34] A. Varela, G. Oliveira, F. G. Souza, Jr., C. H. M. Rodrigues, M. A. S. Costa, *Polym. Eng. Sci.* **2013**, *53*, 44.
[35] E. G. O. Grance, F. G. Souza, Jr., A. Varela, E. D. Pereira, G. E. Oliveira, C. H. M. Rodrigues, *J. Appl. Polym. Sci.* **2012**, *126*, E305.
[36] F. D. Marques, F. G. Souza, Jr., G. E. Oliveira, *J. Appl. Polym. Sci.* **2016**, *133*, 43127.
[37] E. Elias, R. Costa, F. Marques, G. Oliveira, Q. Guo, S. Thomas, F. G. Souza Jr, *J. Appl. Polym. Sci.* **2015**, *132*, 41732.
[38] A. Middea, L. S. Spinelli, F. G. Souza Jr, R. Neumann, T. L. A. P. Fernandes, O. Gomes, F. M. da, *Appl. Clay Sci.* **2017**, *139*, 45.
[39] F. D. Marques, M. Nele de Souza, F. G. Souza, Jr., *J. Appl. Polym. Sci.* **2017**, *134*, 45549.
[40] F. G. Souza, Jr., A. C. Ferreira, A. Varela, G. E. Oliveira, F. Machado, E. D. Pereira, E. Fernandes, J. C. Pinto, M. Nele, *Polym. Test* **2013**, *32*, 1466.
[41] W.-D. Li, J.-B. Zeng, X.-J. Lou, J.-J. Zhang, Y.-Z. Wang, *Polym. Chem.* **2012**, *3*, 1344.
[42] M. I. Khalil, *Arab. J. Chem.* **2015**, *8*, 279.
[43] A. K. Bordbar, A. A. Rastegari, R. Amiri, E. Ranjbakhsh, M. Abbasi, A. R. Khosropour, *Biotechnol. Res. Int.* **2014**, 1.
[44] A. R. Abraham, B. Raneesh, D. Das, N. Kalarikkal, **2016**, 050151.
[45] S. Perumbilavil, K. Sridharan, A. R. Abraham, H. P. Janardhanan, N. Kalarikkal, R. Philip, *RSC Adv.* **2016**, *6*, 106754.
[46] B. Abderrahim, E. Abderrahman, A. Mohamed, T. Fatima, T. Abdesselam, O. Krim, *World J. Environ. Eng.* **2015**, *3*, 95.
[47] Y. Y. Then, N. A. Ibrahim, N. Zainuddin, B. W. Chieng, H. Ariffin, W. M. Z. Wan Yunus, *BioResources* **2015**, *10*, https://doi.org/10.15376/biores.10.2.3577-3601.
[48] M. S. Rajput, P. Agrawal, *Indian J. Cancer* **2010**, *47*, 458.
[49] E. U. X. Péres, M. H. Sousa, F. G. Souza, Jr., F. Machado, P. A. Z. Suarez, *Eur. J. Lipid Sci. Technol.* **2017**, 1600451.
[50] E. D. Pereira, F. G. Souza, Jr., J. C. C. S. Pinto, R. Cerruti, C. Santana, *Macromol. Symp.* **2014**, *343*, 18.
[51] A. Mayeen, M. S., K. Jayalakshmy, M. S. Thomas, S. Rouxel, D. Philip, J. Bhowmik,, N. Kalarikkal, *Dalton Trans.* **2018**, *47*, 2039.
[52] M. Vadivel, R. R. Babu, K. Ramamurthi, M. Arivanandhan, *Nano-Struct. Nano-Objects* **2017**, *11*, 112.
[53] X. Sun, Y. Zheng, L. Sun, Q. Lin, H. Su, C. Qi, *Nano-Struct. Nano-Objects* **2016**, *5*, 7.
[54] A. D. Mani, I. Soibam, *Nano-Struct. Nano-Objects* **2018**, *13*, 59.
[55] G. Anandhababu, G. Ravi, *Nano-Struct. Nano-Objects* **2018**, *15*, 1.
[56] A. L. Glover, J. B. Bennett, J. S. Pritchett, S. M. Nikles, D. E. Nikles, J. A. Nikles, C. S. Brazel, *IEEE Trans. Magn.* **2013**, *49*, 231.
[57] J. van der Zee, *Ann. Oncol. Off. J. Eur. Soc. Med. Oncol.* **2002**, *13*, 1173.
[58] P. Wust, B. Hildebrandt, G. Sreenivasa, B. Rau, J. Gellermann, H. Riess, R. Felix, P. M. Schlag, *Lancet Oncol.* **2002**, *3*, 487.
[59] B. Hildebrandt, P. Wust, O. Ahlers, A. Dieing, G. Sreenivasa, T. Kerner, R. Felix, H. Riess, *Crit. Rev. Oncol. Hematol.* **2002**, *43*, 33.
[60] Z. Behrouzkia, Z. Joveini, B. Keshavarzi, N. Eyvazzadeh, R. Z. Aghdam, *Oman Med. J.* **2016**, *31*, 89.

